

# Ice sheet acceleration driven by melt supply variability

Christian Schoof

Department of Earth and Ocean Sciences, University of British Columbia  
6339 Stores Road, Vancouver, BC, V6T 1Z4, Canada

September 15, 2011

Increased ice velocities in Greenland<sup>1</sup> are contributing significantly to eustatic sea level rise. Faster ice flow has been associated with ice-ocean interactions in water-terminating outlet glaciers<sup>2</sup>, and with increased surface meltwater supply to the ice sheet bed inland. Observed correlations between surface melt and ice speedup<sup>3,2,4,5,6</sup> have raised the possibility of a positive feedback in which surface melting and accelerated dynamic thinning reinforce one another.<sup>7</sup> Here I show that it is not simply mean surface melt<sup>4</sup> but an increase in water input variability<sup>8</sup> that drives faster ice flow. Glacier sliding responds to melt indirectly through changes in basal water pressure.<sup>9,10,11</sup> Observations show that water under glaciers drains through channels at low pressure or through interconnected cavities at high pressure.<sup>12,13,14,15</sup> Using a new model that captures the dynamic switching<sup>12</sup> between channel and cavity drainage modes, I show that channelization and glacier slowdown rather than speedup occur above a critical rate of water flow. Higher rates of steady water supply can therefore suppress rather than enhance dynamic thinning.<sup>16</sup> Short-term increases in water input are however accommodated by the drainage system through temporary spikes in water pressure. It is these spikes that lead to ice speedup, which is therefore driven by strong diurnal melt cycles<sup>14,4</sup> and an increase in rain and surface lake drainage events<sup>17,8,18</sup> rather than an increase in mean melt supply.<sup>3,4</sup>

The effective pressure in the subglacial drainage system, defined as overburden minus basal water pressure, controls coupling between ice and bed: lower effective pressure weakens the ice-bed contact and permits faster sliding.<sup>9,10,11</sup> Effective pressure is controlled by subglacial drainage, which occurs through two principal types of conduits (figure 1): Röthlisberger (R-) channels<sup>19,20</sup> are kept open by a balance between a widening of the channel by wall melting due to heat dissipation in the water flow, and a narrowing that results from the inward creeping motion of the surrounding ice. By contrast, cavities<sup>21,22,11</sup> are formed where ice is forced upward by horizontal sliding over protrusions on the glacier bed. This opens a gap in the lee

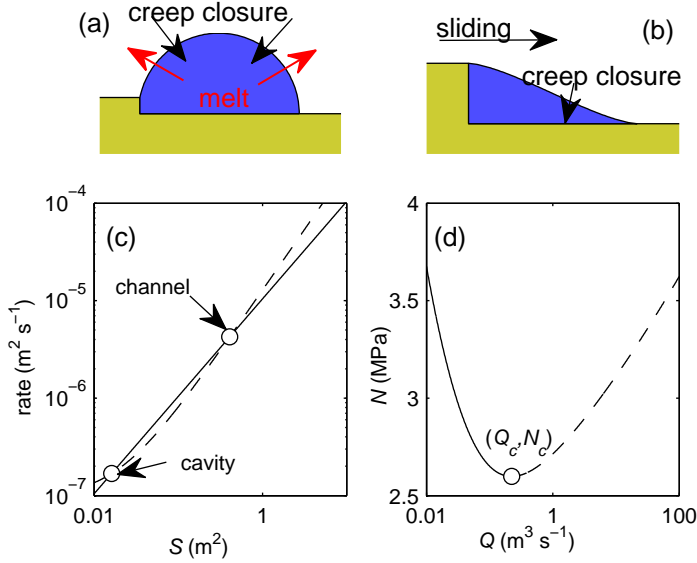


Figure 1: Properties of a single conduit. (a,b): schematics for the physics of channels (a) and cavities (b). (c): Conduit opening rate  $c_1 Q \Psi + u_b h$  (dashed line) and closure rate  $c_2 N^n S$  (solid line) against  $S$  (d): Steady-state  $N$  versus  $Q$  in a conduit (equation (2)). Parameter values are given in the methods summary. Each conduit can generally attain one of two equilibria (points of intersection in (c) given as circles). These can be identified as channel and cavity. The larger (channel) equilibrium is prone to instability:<sup>20</sup> if perturbed to slightly larger size, the conduit will continue to grow (opening rate exceeds closing rate to the right of the intersection). In a network of conduits, this eventually leads to one channel growing at the expense of all other nearby ones. The cavity equilibrium by contrast is stable, and cavities of similar size can co-exist. In steady state, effective pressure increases with discharge in a channel (increased  $N$  makes the closure curve steeper, moving the channel intersection in (c) to larger  $S$ ), and decreases with discharge in a cavity. A conduit becomes a channel above a critical discharge  $Q_c$  (dashed curve in (d)), and remains a cavity below  $Q_c$ .

of the protrusion, with gap size controlled by the opening rate due to sliding and by creep closure of the cavity roof.

An increase in effective pressure leads to faster creep closure. In an equilibrium channel, this must be balanced by greater wall melt. Greater wall melt in turn requires higher discharge and therefore a larger channel. R-channels therefore increase in size with increasing effective pressure (decreasing water pressure). This causes water flow from smaller channels into larger ones, favouring the formation of an arterial network with few main channels at low water pressure.<sup>19,23</sup> Cavities differ from channels as their size is not controlled by wall melt, and increases rather than decreases with water pressure. A reduction in effective pressure suppresses creep closure and allows larger cavities to form.<sup>22,11</sup> This favours macroporous behaviour<sup>24</sup> with spatially distributed drainage along the ice-bed interface and water discharge increasing with water pressure. The presence of channels versus cavities therefore determines whether water pressure is low or high in steady state: channels can efficiently transport water

at high effective pressure, while cavities require low effective pressure to transport the same flux. Past models<sup>23,25</sup> however do not capture switches from cavities to channels in spatially extended drainage or the formation of an arterial network, and cannot predict the spatial configuration of the drainage system.

Here I unify the description of cavities and channels and predict how spatially extended drainage systems can switch from cavities to channels and back. The basic physics of cavities and channels can be captured in a single equation for the cross-sectional area  $S$  of a subglacial conduit, which can be a channel or cavity (see Supplementary Information and figure 1):

$$\frac{dS}{dt} = c_1 Q \Psi + u_b h - c_2 N^n S, \quad (1)$$

where  $Q$  is water discharge,  $\Psi$  is hydraulic gradient along the conduit and  $N = p_i - p_w$  effective pressure in the conduit, equal to ice overburden  $p_i$  minus water pressure  $p_w$ .  $Q$  is related to  $S$  and  $\Psi$  through the Darcy-Weisbach law<sup>26</sup>  $Q = c_3 S^\alpha |\Psi|^{-1/2} \Psi$  where  $\alpha = 5/4$  and  $c_3$  is related to the Darcy-Weisbach friction factor. The first term in (1) is the rate of conduit opening due to wall melting, the second the rate of opening due to sliding of ice at speed  $u_b$  over bed protrusions of size  $h$ , and the third is conduit roof closure due to viscous creep, with  $c_1$ ,  $c_2$  and  $n$  constants related to latent heat of fusion and ice viscosity.

In steady state, effective pressure and discharge in a conduit are then related through (figure 1(d))

$$N^n = \frac{c_1 Q \Psi + u_b h}{c_2 c_3^{-1/\alpha} Q^{1/\alpha} \Psi^{-1/(2\alpha)}}. \quad (2)$$

At low discharge  $Q$ , effective pressure  $N$  drops with  $Q$ , as is expected for cavities, while at higher discharge,  $N$  increases with  $Q$ , and the conduit behaves as an R-channel. The switchover in behaviour occurs at a critical discharge

$$Q_c = \frac{u_b h}{c_1 (\alpha - 1) \Psi}. \quad (3)$$

Below  $Q_c$ , the conduit is mainly kept open by ice flow over bed protrusions, and above  $Q_c$  by wall melting.

A linear stability analysis (see Supplementary Information) also shows that discharge becomes concentrated into a few conduits when mean water discharge through an array of laterally connected conduits exceeds  $Q_c$ : driven by wall melting, a single conduit will grow into a large channel (with the properties of an R-channel, its size  $S$  and effective pressure  $N$  increasing with discharge  $Q$ ) at the expense of nearby ones, which shrink to form smaller cavities. Below this critical mean discharge, all conduits can be stable at the same size and behave as cavities (in which steady-state effective pressure decreases with increasing discharge).

The nonlinear dynamics of channelization can be captured by considering a network<sup>26</sup> of conduits described by (1) (see Methods and Supplementary Information). With mean discharge below a critical value  $Q_c$ , an initially nearly uniform network remains uniform as predicted by linear stability analysis. Above mean discharge level

$Q_c$ , the channelizing instability occurs and the system spontaneously evolves a set of well-defined large channels fed by smaller ones that are separated in turn by cavities (figure 2). This effect is similar to melt channelization in magmatic systems<sup>27</sup>. The spacing between the channels is controlled by lateral effective pressure gradients, and decreases with increasing water input. An important feature of the nonlinear system is that channelization is irreversible. Even if mean discharge is dropped back below  $Q_c$ , the previously formed channels do not necessarily disappear: this requires discharge to drop below a lower critical level  $Q_m$  (figure 2).

An increase in steady meltwater supply lowers effective pressure and therefore speeds up sliding<sup>9,10,11</sup> only below the critical discharge  $Q_c$  for channelization (equation (2), figures 1 (d) and 2 (d)). Once this is exceeded, effective pressure increases again. Channelization increases effective pressure further: concentrated discharge leads to faster channel wall melt that must be offset by stronger creep closure, driven by increased  $N$ . An increase in steady meltwater input therefore has limited potential to cause glacier speed-up, and will eventually even lead to glacier slow-down.

This result however applies only to steady conditions. Observations in Greenland<sup>6</sup> indicate that seasonal and short term water supply variations can lead to transient speedup. Ice velocities in some areas are consistently above their wintertime average early in the melt season, followed by a slowdown to below wintertime average later in summer. This can be explained by a seasonal switch from unchannelized to channelized drainage, in which a combination of elevated water supply and incomplete channelization cause low effective pressures in early summer (figure 3). However, figure 3 also shows that channelization occurs faster and the early melt season drop in effective pressures is smaller when summertime water supply rates are large. Higher summer surface melt rates are therefore likely to suppress the magnitude and duration of the early summer speedup.

Short-term spikes in water supply can also induce spikes in water pressure, and lead to the observed<sup>6</sup> short-term ( $\lesssim 1$  day) fast sliding episodes even when the drainage system has channelized<sup>13</sup> (figure 4). This happens because the size of conduits adjusts slowly (over several days), and the drainage system does not have the capacity to accommodate sudden extra water throughput except by increasing the hydraulic gradient  $\Psi$ . This increase in  $\Psi$  requires higher water pressures in the interior of the drainage system, leading to lower effective pressures and hence to faster sliding. Not only can short term variability lead to speed up even after channelization, but the magnitude of water pressure excursions during short-term water supply spikes can also be much larger than the slower seasonal water pressure signal (compare figures 3(a) and 4(a)).

Ice velocity can therefore respond much more to short-term temporal variations in water supply than to changes in mean water flow. This has major implications for ice sheet dynamics and feedbacks between surface melting and dynamic thinning<sup>7</sup>. More surface water input through melt or rain is likely if dynamic thinning draws down the ice surface. This can lead to increased ice flow and further thinning if basal water supply is initially very low or if the bed is frozen. However, larger rates of summer water supply can also cause faster channelization and potential ice slowdown. Further speedup must then be driven instead by short term temporal variability in

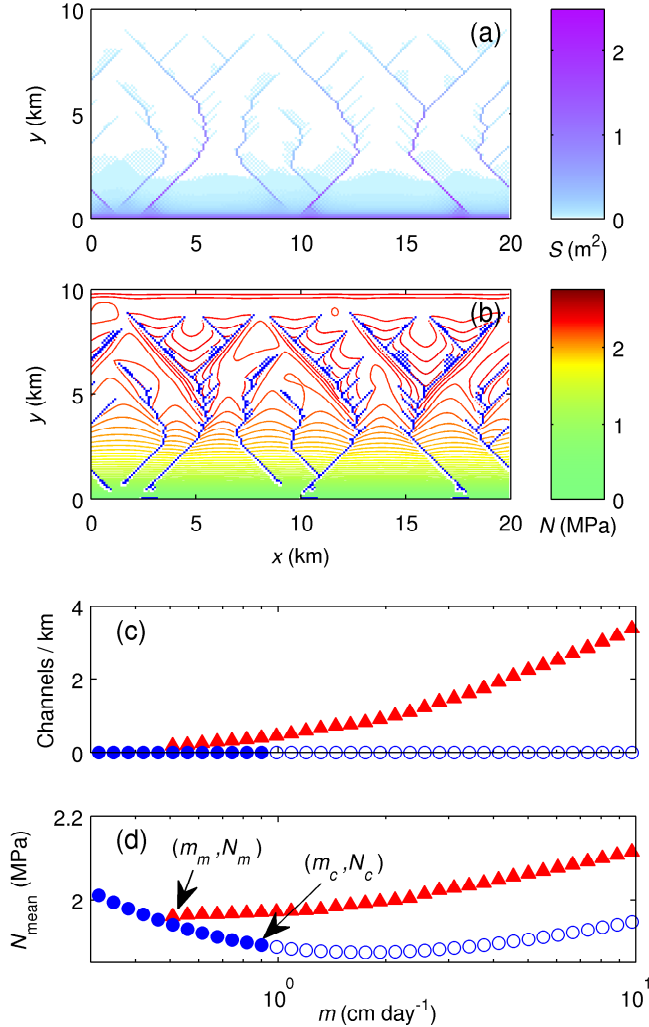


Figure 2: Steady state drainage systems. (a,b): Example of a drainage system formed spontaneously through the channelizing instability. (a) shows conduit sizes. Channels are much larger (dark blue and purple) than the surrounding cavities. (b) shows channels in blue and effective pressure contours at 0.05 MPa intervals. The pressure distribution reveals how channel-cavity interactions control the drainage pattern. Channels are at higher effective pressure than the surrounding cavities. Local water pressure maxima (minima of  $N$ ) separate the channels, driving water flow towards them. (c,d): Steady-state drainage system characteristics as functions of water supply rate  $m$ . (c): channel density (average number of channels per unit width of the domain) against  $m$ . (d): the mean of  $N$  over the domain against  $m$ . Red triangles correspond to channelized systems, blue circles to unchannelized ones. Empty circles show unstable unchannelized systems (which will evolve into a channelized state if perturbed). Instability first occurs at a critical water supply  $m_c$ , corresponding to a critical discharge  $Q_c$ . Mean effective pressure decreases with water supply (and hence discharge) for stable unchannelized systems, and increases with water supply for channelized ones. For some intermediate values of  $m$  (between  $m_c$  and a lower limit  $m_m$  that corresponds to a critical lower discharge  $Q_m$ ), both channelized and unchannelized states are possible: Their low water pressure allows channels to suck in enough water to maintain themselves open, but the discharge through the system is too low for an unchannelized system to channelize spontaneously.

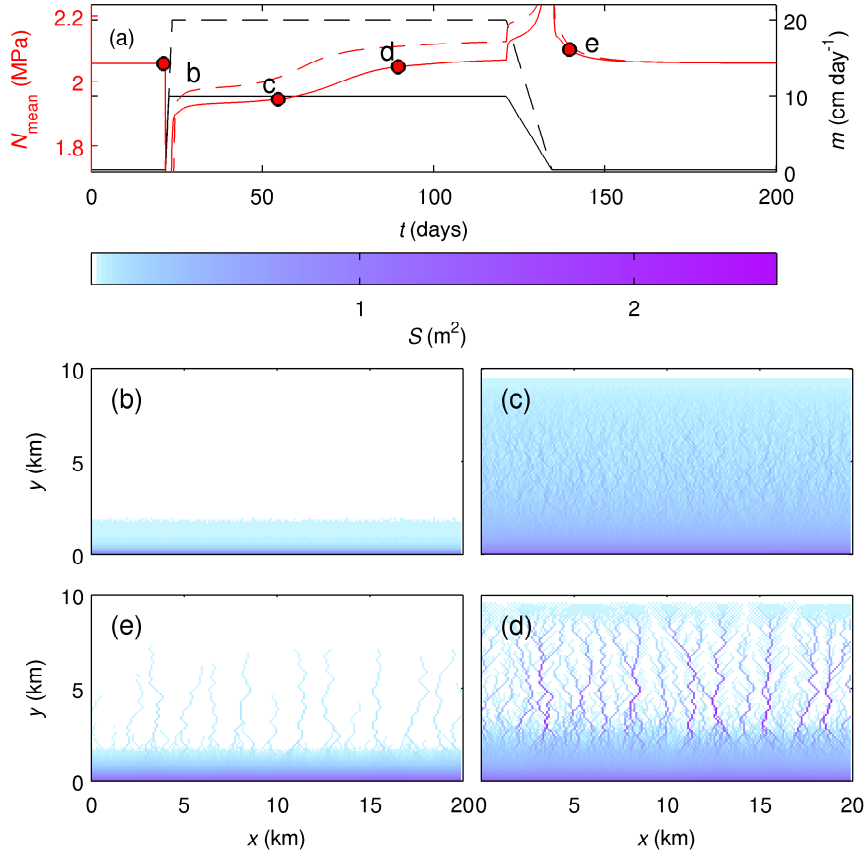


Figure 3: Idealized seasonal evolution of the drainage system. (a): The spatial mean of effective pressure  $N$  (red lines) against time. The simulations shown are forced by a sharp increase (over one day) in water supply  $m$  (black line) from a wintertime value of  $0.33 \text{ cm day}^{-1}$  to a summertime value of  $10 \text{ cm day}^{-1}$  (solid lines) and  $20 \text{ cm day}^{-1}$  (dashed lines). This is followed by steady supply for 100 days and a gradual return to  $0.33 \text{ cm day}^{-1}$ . The dots marked b–e correspond to the spatial drainage configurations shown in panels (b–e), respectively. The drainage system starts close to an unchanneled steady state with small conduits (b). The abrupt increase in  $m$  leads to a sharp drop in effective pressure (a ‘spring event’<sup>9</sup>) which opens the drainage conduits to accommodate the additional discharge, but does not immediately channelize the system (c). Efficient channelization only causes effective pressure to increase after some time (d), reaching above wintertime values. The final drop in  $m$  causes a temporary jump in effective pressure that leads the system to shut down for winter (e). Both simulations in panel (a) show qualitatively the same response. However, the larger jump in water supply (dashed lines in (a)) leads to a shorter and less pronounced period of low effective pressure than the smaller jump (solid lines in (a)). A video animation is included in the Supplementary Information.

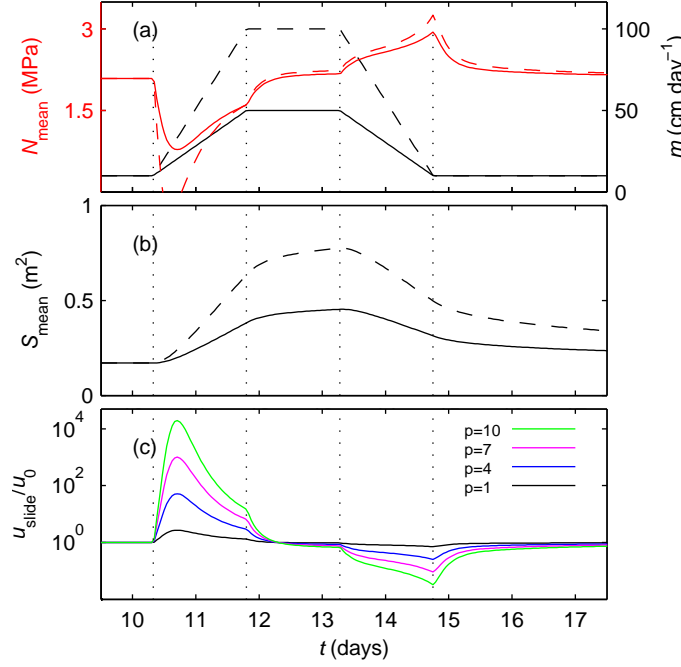


Figure 4: Temporal variations in water input. (a): The mean of  $N$  (red) over the domain against time  $t$  for two different simulations. Simulations are started from a steady state channelized system and forced with time-dependent but spatially uniform water input  $m$  (black), imposing a fivefold (solid lines) and tenfold (dashed lines) increase in  $m$  over 4 days. (b): The spatial mean of conduit size  $S$  against time. During the initial increase in water input, conduits have not yet been able to widen to accommodate increased discharge. To force the additional discharge instead requires a temporary spike in hydraulic gradient  $\Psi$ , leading to higher water pressure (lower  $N$ ) upstream of the margin (red lines). This temporary drop in  $N$  is stronger for bigger jumps in  $m$  (dashed lines in (a)):  $N_{\text{mean}}$  can even drop to zero, which corresponds to complete decoupling between ice and bed. Hydrofracture should occur<sup>30</sup>, though this is not included in my model. After the initial transient, conduit size adjusts and effective pressure increases again, reaching a maximum when  $m$  decreases again. (c): Modelled sliding velocity  $u_{\text{slide}}$  normalized by steady state sliding velocity  $u_0$ . Time series of  $u_{\text{slide}}/u_0$  are shown corresponding to the solid curves in (b) and (c). Sliding is modelled using the empirical relation<sup>9,23</sup>  $\tau_b = C u_{\text{slide}}^{1/p} N$ , where  $\tau_b$  is driving stress in the ice, and  $C$  and  $p$  are constant parameters (see Supplementary Information). The curves correspond to different values of the sliding law nonlinearity  $p$  as indicated. In all cases, the initial drop in  $N$  leads to fast sliding. Recent developments<sup>10,11</sup> in glacier sliding suggest large values of  $p$ , for which the magnitude of sliding events is more pronounced. The calculation for  $u_{\text{slide}}$  however excludes the effects of stress transfer to other parts of the glacier, which would prevent excessively large sliding velocities.

water supply. This is favoured by strong diurnal cycles<sup>5</sup> or frequent rain events,<sup>17</sup> both of which are more likely at lower latitudes, or if the ice sheet develops numerous surface lakes that drain abruptly.<sup>18</sup>

I have developed a new model that captures drainage channelization under glaciers and ice sheets, and shown that this suppresses the ability of steady surface water supply to cause further ice speedup. Accelerated ice flow can be caused instead by water input variations.<sup>8</sup> This is already observable in Greenland, and will become more important under future climate change: diurnal melt cycles already contribute to ice flow in southern Greenland<sup>5</sup>, while more frequent rain events are predicted to result from a northward shift of storm tracks over the next century,<sup>28</sup> which will cause further ice speedup. My results are also relevant to paleo-ice sheet dynamics. Simulations that do not include subglacial processes cannot explain the observed rapid collapse of the Laurentide ice sheet.<sup>29</sup> A water input-dynamic thinning feedback is a plausible collapse mechanism, driven by rain and diurnal melt cycles rather than by mean melt alone. Future coupled models are needed to fully capture the role of drainage in rapid deglaciation, and my results show that channelization and short term drainage variability are the crucial processes that must be captured in these models.

## Methods Summary

I model a drainage network in which nodes  $i$  and  $j$  are connected by a conduit (network edge) labelled by subscripts  $ij$ . The conduit evolves according to

$$\frac{dS_{ij}}{dt} = c_1 Q_{ij} \Psi_{ij} + u_b h - c_2 N_{ij}^n S_{ij}. \quad (4)$$

$S_{ij}$ ,  $Q_{ij}$ ,  $\Psi_{ij}$  and  $N_{ij}$  are conduit size, flux, hydraulic gradient and effective pressure, respectively. Conduit sizes  $S_{ij}$  and effective pressures  $N_i$  at the nodes are the primary variables. I put  $\Psi_{ij} = \Psi_{ij}^0 + (N_j - N_i)/L_{ij}$ , where  $L_{ij}$  is the distance between nodes and  $\Psi_{ij}^0$  a geometrically controlled background hydraulic gradient (see Supplementary Information). Additionally,  $N_{ij} = (N_i + N_j)/2$  and  $Q_{ij} = c_3 S^\alpha |\Psi_{ij}|^{-1/2} \Psi_{ij}$ . At each node, mass is conserved. Ignoring water storage (see Supplementary Information), mass conservation requires

$$\sum_j Q_{ij} = m_i, \quad (5)$$

where the sum is over nodes  $j$  connected to the node  $i$ , and  $m_i$  is water input to node  $i$ . I use a rectangular lattice network oriented at  $45^\circ$  to downslope, with a domain size of  $10 \text{ km} \times 20 \text{ km}$  and  $2 \times 10^4$  conduits. I impose  $N = 0$  at the margin, zero inflow upstream, and periodic sides. Water input is spatially uniform (all  $m_i$  the same), given as  $m =$  rate of volume input per unit area. Parameters are  $\alpha = 5/4$ ,  $c_1 = 3.4 \times 10^{-9} \text{ Pa}^{-1}$ ,  $c_2 = 4.5 \times 10^{-25} \text{ Pa}^{-3} \text{ s}^{-1}$ ,  $c_3 = 0.33 \text{ kg}^{-1/2} \text{ m}^{3/2}$ ,  $u_b h = 3 \text{ m}^2 \text{ year}^{-1}$  (see Supplementary information). For illustrative purposes,  $\Psi_{ij}^0$  is based on the shape of a plastic glacier with yield stress  $10^5 \text{ Pa}$  on a  $3^\circ$  slope. Figure 1 uses  $\Psi = 512 \text{ Pa m}^{-1}$ ,  $u_b h = 3 \text{ m}^2 \text{ year}^{-1}$ , and in panel (c),  $N = 2.85 \text{ MPa}$ .



## References

1. Rignot, E. and Kanagaratnam, P. Changes in the velocity structure of the Greenland ice sheet. *Science* **311**, 986–990 (2006).
2. Joughin, I., Das, S.B., King, M.A., Smith, B.E., Howat, I.M., and Moon, T. Seasonal speedup along the western flank of the Greenland ice sheet. *Science* **320**, 781–783 (2008).
3. Zwally, H.J., Abdalati, W., Herring, T., Larson, K., Saba, J., and Steffen, K. Surface-melt induced acceleration of Greenland ice-sheet flow. *Science* **5579**, 218–222 (2002).
4. van de Wal, R.S.W., Boot, W., van den Broeke, M.R., Smeets, C.J.P.P., Reijmer, C.H., Donker, J.J.A., and Oerlemans, J. Large and Rapid Melt-Induced Velocity Changes in the Ablation Zone of the Greenland Ice Sheet. *Science* **321**, 111–113 (2008).
5. Shepherd, A., Hubbard, A., Nienow, P., King, M., MacMillan, M., and Joughin, I. Greenland ice sheet motion coupled with daily melting in late summer. *Geophys. Res. Lett.* **36**(L01501), doi:10.1029/2008GL035785 (2009).
6. Bartholomew, I., Nienow, P., Mair, D., Hubbard, A., King, M.A., and Sole, A. Seasonal evolution of subglacial drainage and acceleration in a Greenland outlet glacier. *Nature Geoscience* **3**, 408–411 (2010).
7. Parizek, B.R. and Alley, R.B. Implications of increased Greenland surface melt under global-warming scenarios: ice-sheet simulations. *Quat. Sci. Revs.* **23**, 1013–1027 (2004).
8. Bartholomew, T.C., Anderson, R.S., and Anderson, S.P. Response of glacier basal motion to transient water storage. *Nature Geoscience* **1**, 33–37 (2008).
9. Iken, A. and Bindschadler, R.A. Combined measurements of subglacial water pressure and surface velocity of Findelengletscher, Switzerland: conclusions about drainage system and sliding mechanism. *J. Glaciol.* **32**(110), 101–119 (1986).
10. Iverson, N.R., Baker, R.W., Hooke, R.LeB., Hanson, B., and Jansson, P. Coupling between a glacier and a soft bed: I. A relation between effective pressure and local shear stress determined from till elasticity. *J. Glaciol.* **45**(149), 31–40 (1999).
11. Schoof, C. The effect of cavitation on glacier sliding. *Proc. R. Soc. Lond. A* **461**, 609–627, doi:10.1098/rspa.2004.1350 (2005).
12. Kamb, B., Raymond, C.F., Harrison, W.D., Engelhardt, H., Echelmeyer, K.A., Humphrey, N., Brugman, M.M., and Pfeffer, T. Glacier surge mechanism: 1982–1983 surge of Variegated Glacier, Alaska. *Science* **227**(4686), 469–479 (1985).

13. Iken, A., Echelmeyer, K.A., Harrison, W.D., and Funk, M. Mechanisms of fast flow in Jakobshavns Isbrae, Greenland, Part I: Measurements of temperature and water level in deep boreholes. *J. Glaciol.* **39**(131), 15–25 (1993).
14. Hubbard, B., Sharp, M.J., Willis, I.C., Nielsen, M.K., and Smart, C.C. Borehole water-level variations and the structure of the subglacial hydrological system of Haut Glacier d’Arolla, Valais, Switzerland. *J. Glaciol.* **41**(139), 572–583 (1995).
15. Lappégard, G., Kohler, J., Jackson, M., and Hagen, J.O. Characteristics of subglacial drainage system deduced from load-cell measurements. *J. Glaciol.* **52**(176), 137–147 (2006).
16. Magnusson, E., Björnsson, H., Rott, H., and Pálsson, F. Reduced glacier sliding caused by persistent drainage from a subglacial lake. *The Cryosphere* **4**, 13–20 (2010).
17. Howat, I.M., Tulaczyk, S., Waddington, E., and Björnsson, H. Dynamic controls on glacier basal motion inferred from surface ice motion. *J. Geophys. Res.* **113**(F03015), doi:10.1029/2007JF000925 (2008).
18. Das, S.B., Joughin, I., Behn, M.D., Howat, I.M., King, M.A., Lizarralde, D., and Bhatia, M.P. Fracture propagation to the base of the Greenland ice sheet during supraglacial lake drainage. *Science* **320**, 778–781 (2008).
19. Röthlisberger, H. Water pressure in intra- and subglacial channels. *J. Glaciol.* **11**(62), 177–203 (1972).
20. Nye, J.F. Water flow in glaciers: jökulhlaups, tunnels and veins. *J. Glaciol.* **17**(76), 181–207 (1976).
21. Walder, J. Hydraulics of subglacial cavities. *J. Glaciol.* **32**(112), 439–445 (1986).
22. Kamb, B. Glacier surge mechanism based on linked cavity configuration of the basal water conduit system. *J. Geophys. Res.* **92**(B9), 9083–9100 (1987).
23. Fowler, A.C. Sliding with cavity formation. *J. Glaciol.* **33**(105), 255–267 (1987).
24. Lüthi, M., Funk, M., Iken, A., Gogineni, S., and Truffer, M. Mechanisms of fast flow in Jakobshavns Isbrae, Greenland; Part III: measurements of ice deformation, temperature and cross-borehole conductivity in boreholes to the bedrock. *J. Glaciol.* **48**(162), 369–385 (2002).
25. Hewitt, I.J. and Fowler, A.C. Seasonal waves on glaciers. *Hydrological Processes* **22**, 3919–3930 (2008).
26. Clarke, G.K.C. Lumped-element analysis of subglacial hydraulic circuits. *J. Geophys. Res.* **101**(B8), 17547–17559 (1996).
27. Hewitt, I.J. and Fowler, A.C. Melt channelization in ascending mantle. *J. Geophys. Res.* **114**(b06210), doi:10.1029/2008JB006185 (2009).

28. Schuenemann, K.C. and Cassano, J.J. Changes in synoptic weather patterns and greenland precipitation in the 20th and 21st centuries: 2. analysis of 21st century atmospheric changes using self-organizing maps,. *J. Geophys. Res.* **115**(D05108), doi:10.1029/2009JD011706. (2010).
29. Tarasov, L. and Peltier, W.R. Terminating the 100 kyr ice age cycle. *J. Geophys. Res.* **102**(D18), 21665–21693 (1997).
30. Tsai, V.C. and Rice, J.R. A model for turbulent hydraulic fracture and application to crack propagation at glacier beds. *J. Geophys. Res.* **115**(F03007), doi:10.1029/2009JF001474 (2010).

**Supplementary Information** is linked to the online version of the paper at [www.nature.com/nature](http://www.nature.com/nature).

**Acknowledgements:** Thanks to Garry Clarke, Tim Creyts, Gwenn Flowers, Ian Hewitt, Richard Hindmarsh, Mark Jellinek and Valentina Radić for comments on the manuscript, and to Conrad Koziol and Marc Jaffrey for discussions. Financial support was provided by the Canada Research Chairs Program, NSERC Discovery Grant 357193-08, and the Canadian Foundation for Climate and Atmospheric Science through the Polar Climate Stability Network.

**Author Information:** Reprints and permissions information is available at [npg.nature.com/reprintsandpermissions](http://npg.nature.com/reprintsandpermissions). Correspondence and requests for materials should be addressed to [cschoof@eos.ubc.ca](mailto:cschoof@eos.ubc.ca).

**Competing financial Interests:** The author declares that he has no competing financial interests.